npj | quantum information

Article

Published in partnership with The University of New South Wales

https://doi.org/10.1038/s41534-024-00899-6

Many-body entanglement via 'which-path' information

Ron Ruimy[1,3], Offek Tziperman[1,3], Alexey Gorlach[1], Klaus Mølmer[2] & Ido Kaminer[1]

We propose a multi-particle 'which-path' gedanken experiment with a quantum detector. Contrary to conventional 'which-path' experiments, the detector maintains its quantum state during interactions with the particles. We show how such interactions can create an interference pattern that vanishes on average, as in conventional 'which-path' schemes, but contains hidden many-body quantum correlations. Measuring the state of the quantum detector projects the joint-particle wavefunction into highly entangled states, such as GHZ's. Conversely, measuring the particles projects the detector wavefunction into desired states, such as Schrodinger-cat or GKP states for a harmonic-oscillator detector, e.g., a photonic cavity. Our work thus opens a new path to the creation and exploration of many-body quantum correlations in systems not often associated with these phenomena, such as atoms in waveguide QED and free electrons in transmission electron microscopy.

The double-slit experiment with matter waves (Fig. 1a) is one of the most famous experiments in the history of physics[1–4]. A core concept behind the double-slit experiment is 'which-path' information (Fig. 1b). Any attempt to observe the path taken by a particle will inhibit it from forming an interference pattern[5]. The 'which-path' concept became the textbook example of complementarity in quantum mechanics, i.e., the inability to simultaneously measure certain properties of quantum systems, such as a particle's position and momentum. '

The story of 'which-path' information was later connected to weak measurements[6]. When a measurement device (i.e., detector) provides partial information about a particle trajectory, for example via a weak interaction, it does not fully inhibit the formation of the interference pattern but instead decreases its visibility[7]. Many other variants of 'which-path' experiments have been proposed, such as delayed choice[8] and quantum eraser[9,10] experiments. These works and many others highlight many of the mysteries of quantum mechanics, and as popularized by Feynman: "it (the double-slit experiment) contains the *only* mystery"[11].

However, there is a key ingredient to quantum mechanics missing from the conventional which-path experiment: quantum entanglement. The conventional experiment concerns the measurement of single-particle observables, whereas observing entanglement requires the measurement of multi-body correlations[12].

Here we propose a multi-particle which-path experiment, revealing many-body correlations that can be created using the universal concept of 'which-path' information. We show what operations create multi-particle entanglement in the limited space of symmetric states[13], and what operations reach the full exponentially large many-body Hilbert space.

At the heart of every 'which-path' experiment lies the measurement of the path, which causes the collapse of the particle trajectory due to its interaction with the detector. The detector's state becomes entangled with the particle's trajectory. We show that if the detector preserves its quantum state between its interactions, the trajectories of the different particles can collectively interfere. Then, although the interference pattern still vanishes on average, strong quantum correlations between the particles emerge.

The concept we propose applies to a wide range of quantum systems. Fig. 1 illustrates this concept, depicting a double-slit setup together with the analogous quantum circuit. We compare three options. Fig. 1a1: conventional interference pattern with no detector, Fig. 1b1: conventional 'which-path' with a classical detector that destroys the interference, and Fig. 1c1: a quantum detector that preserves coherence between interactions and thus creates multi-particle quantum correlations.

The analog quantum circuit represents the two paths of the particle using qubit states $|0\rangle$ and $|1\rangle$. The splitting and interference of the trajectories are represented by Hadamard gates. The two orthogonal final interference patterns are identified using $|0\rangle$ and $|1\rangle$ after the Hadamard gate, with $|0\rangle$ being the ordinary interference pattern without the detector. The detector's 'which-path' measurement is a conditional operator that entangles the detector with the particle. To model the conventional 'which-path' experiment, we reset the detector state after interacting with each particle. The reset randomizes the particle measurement outcomes and diminishes the interference pattern. In contrast, if the detector preserves its quantum state between interactions with all the particles, their measurement outcome becomes correlated.

We consider two quantum detector models: either a fermionic or a bosonic system. The former is a qubit state describing a binary "yes/no"

[1]Solid State Institute, Technion-Israel Institute of Technology, Haifa, 32000, Israel. [2]Niels Bohr Institute, Univesity of Copenhagen, Blegdamsvej 17, 2100 Copenhagen, Denmark. [3]These authors contributed equally: Ron Ruimy, Offek Tziperman. e-mail: kaminer@technion.ac.il

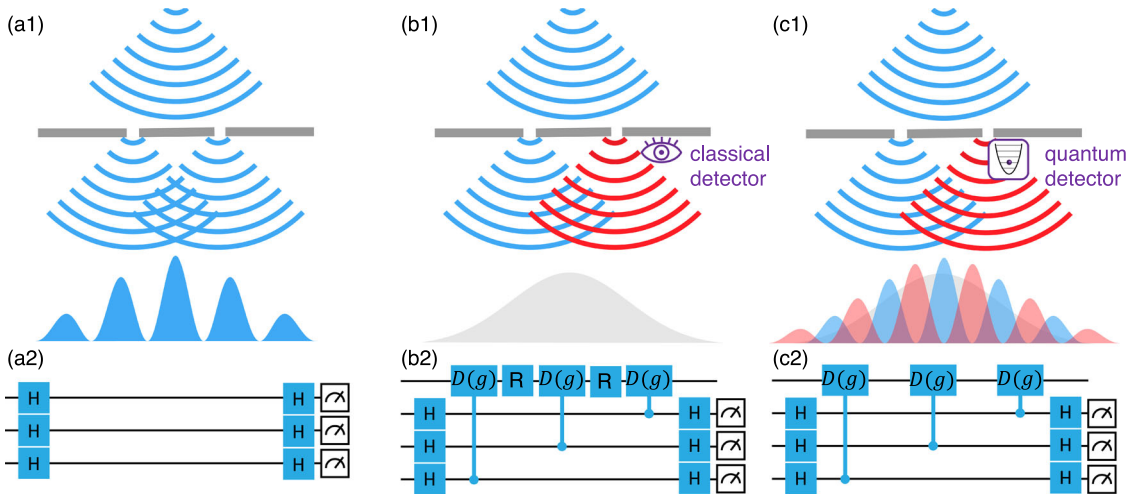

Fig. 1 | The multi-particle 'which-path' experiment: implementations in double-slit setups, with analog quantum circuit representations. (a1). Conventional `which-path' experiment: with no detector, the particle is split into two paths that are later combined, creating an interference pattern. **a2** The Hadamard $H$ gate represents both the splitting and combining of the paths. **b1** Conventional `which-path' experiment: a classical detector in one of the paths destroys the interference pattern. **b2** The detection can be modeled using a unitary operator changing the detector state conditioned on the particle state. Each R gate resets the detector state such that it has no memory. **c1** `Which-path' experiment with a quantum detector: the detector interaction entangles it with the particles, resulting in multi-particle quantum correlations. **c2** Without the R gates, the detector correlates the particles because its state is maintained between its interactions with them. The detector can be modeled by conditional gates such as CNOT for a qubit detector or conditional displacement for a harmonic-oscillator detector. The latter case is analyzed below, denoted by $D(g)$ with interaction strength g, describing for example a photonic cavity.

measurement outcome. The latter is a quantum harmonic oscillator describing a photonic or a vibrational mode excited by the particle. The fermionic detector implements a Pauli X gate, and then the 'which-path' experiment generates the highly entangled Greenberger-Horne-Zeilinger state[12]. The bosonic detector implements a conditional displacement, and then the 'which-path' experiment generates a many-body quantum walk[13].

We focus below on the bosonic detector, which could be implemented in a wide range of systems. We exemplify the implications using two concrete systems: quantum emitters such as atoms or quantum dots emitting light into a common mode, such as a waveguide or cavity[14,15], or free electrons interacting with a cavity before interfering in a transmission electron microscope (TEM)[3]. In both systems, we show how to create many-body correlations and how to control the corresponding detector state, for the generation of desired quantum photonic states.

Results

Quantum circuit model

The interaction of each particle with the detector's harmonic oscillator state can be modeled using a conditional displacement operator[16]:

$$\begin{aligned} CD(g) &= I \otimes |0\rangle\langle 0| + D(g) \otimes |1\rangle\langle 1| \\ D(g) &\equiv e^{ga^\dagger - g^* a}. \end{aligned} \tag{1}$$

Here, $|0\rangle$,$|1\rangle$ are the particle states corresponding to the different paths, and $a^\dagger$, a are the creation and annihilation operators that act on bosonic detector states denoted by $|\rangle_{\mathrm{ph}}$. The displacement operator $D(g)$[17] depends on the particle-detector interaction strength represented by the (complex) parameter g, satisfying $D(g)|\alpha\rangle_{\mathrm{ph}} = |\alpha + g\rangle_{\mathrm{ph}}$ for every coherent state $|\alpha\rangle_{\mathrm{ph}} \equiv e^{-\frac{|\alpha|^2}{2}} \sum_{n=0}^{\infty} \frac{\alpha^n}{\sqrt{n!}} |n\rangle_{\mathrm{ph}}$, with $|n\rangle_{\mathrm{ph}}$ being the number states.

A classical detector is modeled by applying the gates $H \cdot CD(g) \cdot H$ on the joint particle-detector wavefunction and then tracing out its state. Then, using the formula for the inner-product of two coherent states $\langle\beta|\alpha\rangle = e^{-\frac{1}{2}(|\alpha|^2 + |\beta|^2 - 2\beta^*\alpha)}$[17], the final state of each particle becomes a mixed density matrix:

$$\rho_f = \frac{1}{2} \begin{pmatrix} 1 + e^{-\frac{1}{2}|g|^2} & 0 \\ 0 & 1 - e^{-\frac{1}{2}|g|^2} \end{pmatrix}. \tag{2}$$

The purity of this state is $\gamma_f = tr(\rho_f^2) = \frac{1}{2} + \frac{1}{2} e^{-|g|^2}$. As $|g|$ increases, the state transitions from completely pure (perfect interference fringes, weak or no detection) to completely mixed (no fringes, strong detection). For strong detection (large $|g|$), the chance to measure all the k particles in the original fringe (state $|0\rangle$) is exponentially small in the number of particles $\left(2^{-k}\right)$.

Creating the many-body quantum state

We now consider the same experiment but with the quantum detector. The final joint particle-detector state is $|\psi_f\rangle = \left(H \cdot CD(g) \cdot H\right)^{\otimes k} |0\rangle^{\otimes k} |0\rangle_{\mathrm{ph}}$. It is convenient to define the non-unitary operators $C_\pm \equiv \frac{1}{2}(I \pm D(g))$, in which case the final state can be written as:

$$|\psi_f\rangle = \sum_{n=0}^{k} \sum_{\mathrm{perm}} |0\rangle^n |1\rangle^{k-n} \otimes C_+^n C_-^{k-n} |0\rangle_{\mathrm{ph}}. \tag{3}$$

Formally, $\sum_{\mathrm{perm}}$ represents the sum over all unique sequences $|s_1 s_2 \ldots s_k\rangle$ where each s_i is either 0 or 1, and the total number of zeros is n and the total number of ones is $k - n$. The probability to measure n particles in the state $|0\rangle$ and $k - n$ particles in the state $|1\rangle$ is then (SM1.1):

$$P_{n,k-n} = \frac{(-1)^n}{4^k} \binom{k}{n} \sum_{j=0}^{2n} \sum_{i=0}^{2(k-n)} \binom{2n}{j} \binom{2(k-n)}{i} (-1)^j e^{-\frac{1}{2}|g|^2 |k-i-j|^2}. \tag{4}$$

This process is akin to a random walk with quantum coin tosses[13,18] deciding whether to displace the detector state at each step. The same final state is reached through different paths, i.e., different sequences of displacements. These paths constructively interfere and thus, for strong interactions, the probability of measuring all k particles in the same final

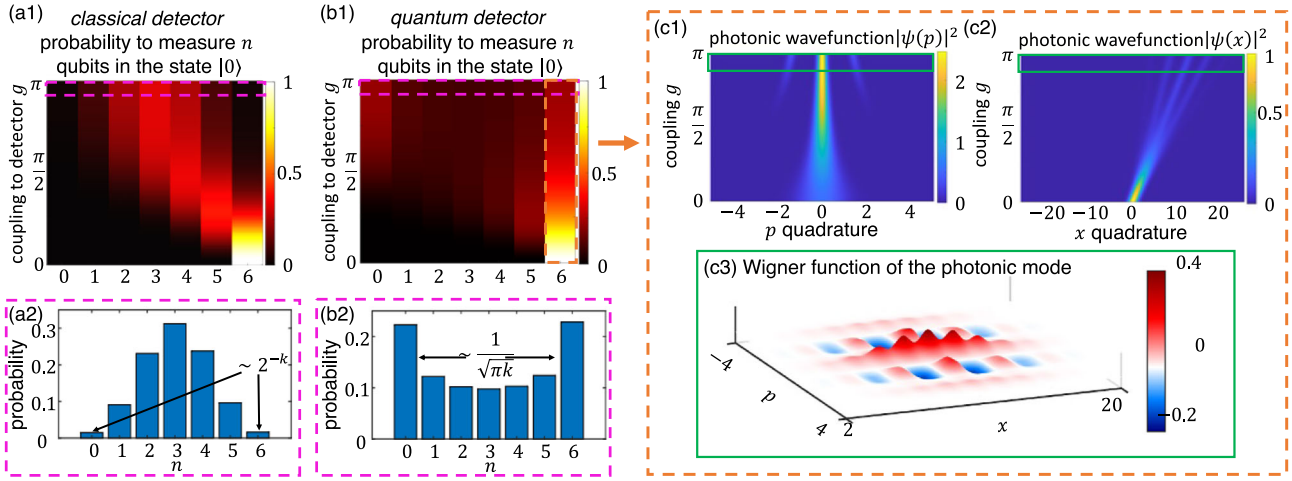

Fig. 2 | Quantum correlations in the particles and in the detector. (a,b). Particle correlations: Comparing the "which-path" variants with classical (**a**) and quantum (**b**) detectors. The probability to measure n of the total $k = 6$ particles in the $|0\rangle$ state is presented as a function of the particle-detector coupling strength g (**a1**, **b1**), showing strong anti-correlations in the limit of strong coupling (**a2**, **b2**). **c** Detector correlations: The state of the quantum detector (a quantum harmonic oscillator) presented in the p (**c1**) and x (**c2**) quadratures, as a function of the coupling strength, post-selected on all particles measured in the $|0\rangle$ state. The Wigner function in the limit of strong coupling (**c3**) is highly non-Gaussian, taking the form of a (GKP-like) grid of coherent states.

state is approximately $\frac{1}{\sqrt{\pi k}}$ (see methods), which strongly amplifies the exponentially small probability of the classical detector. The mathematical reason for this interference can be understood from the norm of the operator $C_+^n C_-^{k-n}$, which equals $\sqrt{\frac{n^n(k-n)^{(k-n)}}{k^k}}$ (see methods). The norm is maximal when $n = 0, k$ and minimal when $n = k/2$, implying that there is a tendency for the particles to bunch together in one output or in the other. This bunching holds resemblance to bosonic interference phenomena although the particles in our description are distinguishable (either in temporal or spatial degrees of freedom). The bosonic behavior can be understood from the fact that the detector state is symmetric to permutations of the particles, resulting in boson-like interference.

To illustrate the implication of this result, we consider repeating this which-path experiment many times, each with $\sim k = 100$ particles. Both classical and quantum detectors will show no interference pattern on average. However, *in each repetition of the experiment*, all the $k = 100$ particles will form the same fringe with a probability >0.1 using a quantum detector rather than 10^{-30} using a classical detector.

The paths of each particle can be described as a spin 1/2 system, and the total state of N particles that are symmetric to permutation can be described in the subspace of maximal total angular momentum or *Dicke states*[14]. The key component that creates the many-body correlations is a non-destructive measurement of the angular momentum projection, i.e., how many particles pass through each path. Similar correlations can be obtained by measuring in this basis with a classical detector, albeit this cannot create quantum photonic states in the detector (still, previous works showed that such a detection can entangle particles[19–22]).

Since the operator $CD(g)$ is fully entangling in the limit of $g \gg 1$, by measuring the detector's final state, the particles' state can collapse into an entangled state. For example, for $k = 2$, measuring the detector will give a Bell state or a Hadamard state, with a 50% − 50% chance (see methods). Bell states are important resources for quantum metrology, providing precision beyond the standard quantum limit[23], as is one of the goals of quantum electron microscopy[24–28]. Going beyond $k = 2$ can create more complex entangled states, similar to N00N states, which can provide Heisenberg-limited scaling for quantum metrology[23]. We note that the state of the quantum detector can be indirectly measured using post-selection on additional particles.

To prove the entanglement of the multi-particle state, we can control the particle interferometry (the final Hadamard gate): measuring the particles in orthogonal bases will break a Bell inequality. For example, measuring the particle states before and after applying the final Hadamard gate, will show correlations that are unobtainable classically.

Furthermore, adjusting the relative phase of the coherent displacements (phase of g), can break the symmetry between the particles. This can be done by tuning the relative arrival time of the particles in the optical cycle. This way we can control the complex quantum state of multiple particles, tapping into the vast potential of their exponential Hilbert space. By controlling the initial conditions and studying the emergent dynamics, our multi-particle 'which-path' implements a quantum simulator.

The detector's quantum state

The 'which-path' experiment can be used to control the quantum state of the detector. If n particles are measured in the state $|0\rangle$ and k-n in the state $|1\rangle$, then the detector state is $|\psi_f\rangle_{\rm ph} \propto C_+^n C_-^{k-n}|0\rangle_{\rm ph}$. This state can be highly non-Gaussian. If the k particles are measured in $|0\rangle$, the final state takes the form of a 1D grid of coherent states:

$$|\psi_f\rangle_{\rm ph} \propto \sum_{n=0}^{k} \binom{k}{n} |(k-n)\rangle_{\rm ph}. \tag{5}$$

Figure 2c shows the Wigner function[29] of this state for $g = \pi$, and its x and p quadrature representations as a function of g. The detector state transitions from a Gaussian squeezed state to a non-Gaussian grid state for larger g values. Our scheme can create a Gottesman-Kitaev-Preskill (GKP) detector's state[30] up to Gaussian operations. For a GKP state with squeezing r, we can take $g = \sqrt{2\pi}e^r$. The goal of 10dB squeezing, a threshold for fault-tolerant quantum computation[31], requires 3 particles with $r = 3$, and then the post-selection probability to create this GKP state is 31.3% (see methods)[32].

We find that the limit of weak g creates a squeezed vacuum state[17] with squeezing of $r = \frac{1}{2}\ln\left(\frac{k|g|^2}{2} + 1\right)$. The probability to post-select this state depends only on the squeezing, rather than on the number of particles, and is equal to e^{-r} (see methods). For larger g values, already a single particle deterministically generates a Schrodinger cat state of the form $|\psi_f\rangle \propto |0\rangle_{\rm ph} \pm |g\rangle_{\rm ph}$ where the ±sign is decided by the particle measurement outcome ($|0\rangle$ or $|1\rangle$).

Physical implementations

This section proposes two implementations of the multi-particle 'which-path' experiment. The first is an electron holography setup[33–35] with a

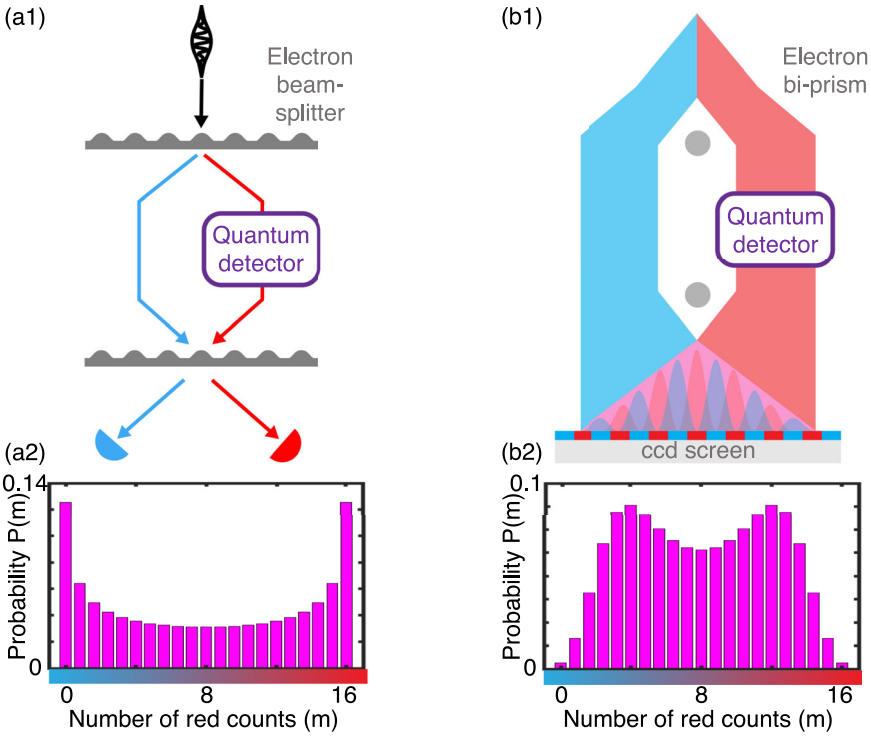

Fig. 3 | Implementation of the multi-particle 'which-path' scheme using split-illumination off-axis electron holography. The setup splits and then combines back an electron beam. A microwave cavity is placed in one of the paths. The two paths interfere either on a two-port beam-splitter (**a1**) or on screen (**b1**) divided into colored sections that denote the two-port outputs. The beam-splitter output results in pronounced anti-correlated distribution (**a2**), while the inerference on a screen result in a less pronounced but still clear anti-correlated distribution (**b2**).

microwave cavity in one of the paths, resembling the typical image of a double-slit setup (Fig. 3). The second is a waveguide-QED setup in which multiple emitters interact with the same mode (Fig. 4). In this case, the "paths" are taken by electrons of the emitters in different internal states.

Any implementation requires the realization of two components with sufficiently high fidelity: (1) Hadamard gate: To combine or separate the particle states into two distinct states representing the logical states. (2) Conditional displacement gate: State-selective interaction between the particle and the detector, displacing the detector state without back-action on the particle.

Our first proposed implementation. relies on split-illumination holography[36] in a transmission electron microscope (Fig. 3b). Denoting the electron's left and right paths by $|0\rangle$ and $|1\rangle$, their interference creates the fringe pattern that corresponds to the state $|0\rangle + |1\rangle$. The orthogonal state is the fringe with a quarter of a wavelength offset that corresponds to the state $|0\rangle - |1\rangle$. Then, dividing the measurement screen into equal sections quarter wavelength apart enables observing the correlation between the final states of the electrons. Fig. 3b shows that the overlap between the fringes limits their distinguishability, smearing the measured anti-correlations (see methods and ref. 37).

Figure 3a shows that using an electron beam-splitter to convert the fringes into separate paths creates more pronounced anti-correlation. The electron beam-splitter can be realized in many different ways such as crystals[38,39], diffraction gratings[40], and more advanced phase masks[41], each with different pros and cons like limited fidelity. Additional proposed realizations include laser[42] or microwave[43] fields and electron mirrors[44]. The electron beam-splitters could be optimized to have two inputs and outputs, as expected from true Hadamard gates. The electron beam-splitters can also be used for splitting the electron before the cavity interaction (e.g., instead of a bi-prism). There, the electron beam-splitter should not be optimized for fidelity but used to provide round spot size enabling precise electron beam overlap and better transverse coherence. If the initial beam-splitter is lossy or has more than two outputs, then they can be eliminated by measuring them, essentially post-selecting only electrons that passed through the desired outputs. In the second electron beam-splitter, this could not be tolerated as lost electrons destroy the many-body entanglement.

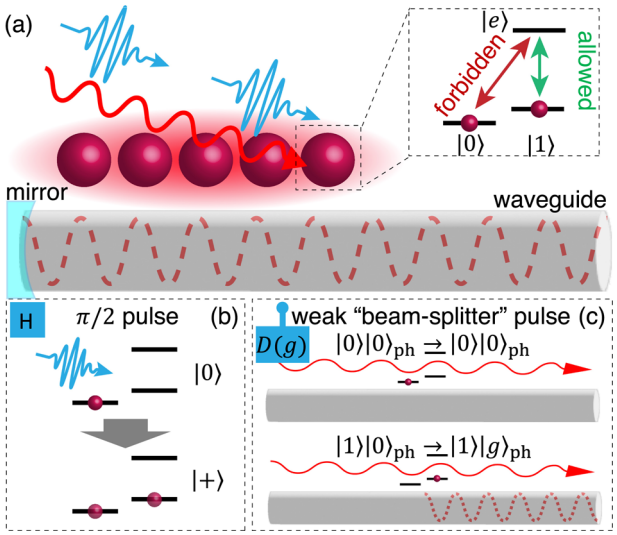

Fig. 4 | Implementation of the multi-particle 'which-path' scheme using waveguide-QED with quantum emitters such as atoms in a Λ configuration. One of the electronic transitions couples to the driving laser (**a**). The two ground states represent the two "paths", $|0\rangle$ and $|1\rangle$. Coherent control pulses act as Hadamard gates (**b**). Weak illumination pulses couple each emitter in the correct state to the waveguide, creating a conditional displacement (**c**).

For this implementation to work, the quantum detector must satisfy several conditions: (1) The cavity lifetime (T_1) and coherence time (T_2) should be long enough such that it interacts with all the electrons before losing the quantum nature of its state. (2) The cavity should be cooled to limit thermal fluctuations. (3) The coupling strength g of the electron with the photonic mode should be strong enough, with $g = \frac{ie}{2\hbar\omega}\int_{-\infty}^{\infty} E_z^{\mathrm{vac}}(z)e^{i\omega z/v}dz$ integrating the cavity vacuum field E_z^{vac} along the electron trajectory in one of its paths. (4) A single-mode of the cavity should dominate its interaction with the electron, meaning that the modes are well

isolated and that the other modes are only weakly coupled to the electrons, for example, due to different phase-matching conditions[45]. (5) All the electrons arrive either at the same time to the detector, or periodically in time such that they are locked with the cycle of the mode. (6) The photonic mode frequency ω should be of sufficiently low such that it does not induce back-action on the electron, i.e., satisfying $\omega \ll \frac{v}{(kg)^2\sigma_z}$, where k is the number of electrons, v is the electron velocity and σ_z is the spatial extent of the free-electron wavepacket along its direction of motion z (see methods). (7) The electron is paraxial, and its energy is much higher than that of the photon, implying that the scattering matrix describing their interaction is given by[46,47] (see methods and[48]):

$$S = e^{ge^{\frac{i\omega}{v}}za^\dagger - g^* e^{-\frac{i\omega}{v}}za}. \tag{6}$$

and can be reduced to the ordinary displacement operator by assuming negligible photon back-action.

Condition (3) is especially challenging, yet critical for strong entanglement. In recent years substantial effort has been invested to increase the coupling between electrons and photonic modes, primarily in the optical regime, to achieve single-electron-single-photon coupling ($g \sim 1$)[45,49,50]. Due to their higher flexibility in design, microwave cavities could lead to breakthroughs in this regard as we recently investigated[51].

Our interferometry proposal closely relates to the works of Okamoto[24–26], who proposed interferometry of electrons that strongly interact with superconducting qubits. There, the electrons get entangled to such qubits, creating GHZ states. Our work also relates to interference experiments of electrons passing nearby semiconductors and metallic surfaces, interacting with the electron gas inside them[52,53], showing a controllable washing-out of the interference pattern. In contrast to our work, in such experiments, the electron emits distinguishable photons, acting as a classical detector. All these experiments could be viewed as part of the general family of which-path experiments, with various types of detectors. Our work shows how all these experiments can lead to the phenomena of many-body quantum correlations.

Our second proposed implementation. relies on k emitters such as atoms coupled to a 1D waveguide (Fig. 4)[15]. In this case, the "two paths" $|0\rangle$, $|1\rangle$ of our scheme are two hyperfine levels of each emitter.

The Hadamard gate can be implemented via a microwave $\pi/2$ pulse resonant with the $|0\rangle$ to $|1\rangle$ transition or using Stimulated Raman Adiabatic Passage[54]. Then, by turning on a laser tuned for the transition between the state $|1\rangle$ and an excited state $|e\rangle$, the emitters begin to populate the excited state and radiate into the waveguide. We assume that the transition $|0\rangle \leftrightarrow |e\rangle$ is forbidden by detuning or selection rules, and in this case, emission into the waveguide is conditioned on the internal state of the emitters ($|0\rangle$ or $|1\rangle$). In the limit where the Rabi frequency associated with the optical transition $|1\rangle \leftrightarrow |e\rangle$ satisfies $\Omega_R \ll k\Gamma_{1D}$ (where Γ_{1D} is the decay rate into the waveguide), the emitters are in their linear regime, and the radiation emitted is a coherent state $|\alpha\rangle$ in a single temporal mode. The magnitude of α scales as the number of emitters occupying the state $|1\rangle$ (see SM3.2 for full derivation).

At the end of the process, the number of emitters in each hyperfine state can be measured to herald particular photonic states (indirect post-selection emitter measurements are possible by subsequent excitations). The system should satisfy a few conditions to effectively implement the protocol: (1) The collective decay rate into the waveguide should be sufficiently greater than the decay rate into free space $\Gamma_{1D} \gg \Gamma'$. (2) The emitters remain in their linear regime ($\Omega_R \ll k\Gamma_{1D}$). (3) The dephasing time T_2^* must be far larger than the total protocol time. When all these conditions are met, the laser implements a conditional displacement between the qubit of the hyperfine state and the propagating pulse in the waveguide.

For a single emitter, the protocol creates the state $|\psi\rangle \propto |0\rangle_e(|0\rangle + |\alpha\rangle_{v(t)}) + |1\rangle_e(|0\rangle - |\alpha\rangle_{v(t)})$, where the indices e, $v(t)$ are for the emitter and photonic state in temporal mode $v(t)$ which, in the linear regime (see SM3), matches the temporal shape of the driving fieldw. By measuring the internal state of the emitter, its emission is heralded into a cat state. Cat states with large photon numbers are desired for various applications, yet are very challenging to create, especially in the optical range. The maximum magnitude of α that can be achieved is approximately determined by the amplitude of the field emitted to the waveguide mode in the typical timescale of the decoherence channel (full analysis given in the SM3.4 and in refs. 55–60):

$$\alpha \approx \min\left\{\sqrt{\Gamma_{1D}/\Gamma'}, \sqrt{\Gamma_{1D}T_2^*}\right\}. \tag{7}$$

Discussion

Our work describes a multi-particle 'which-path' experiment with a detector that interacts with multiple particles while maintaining its quantum state. We find that the particles develop strong correlations due to their path interference. Moreover, measuring the particles generates useful detector states (e.g., cat and GKP photonic states), whereas measuring the detector creates useful entangled particle states. The special case of a fermionic detector that contain a discrete 'yes/no' degree of freedom rather than a full harmonic oscillator can capture a range of schemes used for generating multi-partite entanglement: Consider a quantum detector described by conditional gates (such as CNOT or Controlled Phase gates). In this case, the "path" is encoded on the state of the control qubit, and the detection is performed via an entanglement with the controlled qubit. Such operations are routinely used to generate multi-partite entanglement in quantum information platforms such as superconducting qubits[61] and atom-cavity systems[62]. Our gedanken experiment thus provides a description of such experiments in the language of 'which-path' information.

So far, we have shown how to reach entangled particle states in the effective Hilbert space of symmetric states. However, the interactions in any many-body which-path scheme can reach the entire exponentially large Hilbert space. The way to reach the entire Hilbert space we can break the symmetry between the particles, for example, by shifting the arrival time of the electrons relative to the optical cycle, or by shifting the positions of the emitters along the waveguide. This approach can create more complicated entanglement structures. For example, the shift of the electron arrival time or emitters position by half the mode cycle creates destructive (rather than constructive) interference between two consequent particles, completely altering the correlations. Another way to access the exponentially large Hilbert spaces is to use a multi-mode quantum detector or multiple detectors.

Due to the universality of the "which-path" concept, our method could potentially be implemented in many physical systems such as trapped ions coupled to joint vibrational modes[63–65], arrays of superconducting qubits[66,67], quantum dots[68], atoms in tweezers[69,70] coupled to a waveguide or to a cavity, atomic ensembles probed by off-resonant light[19,21,22], interferometric experiments with various free particles[3,4], and various schemes relying on single-photon nonlinearities[71].

Methods

Quantum circuit model

In the case of a single particle, following the quantum circuits as in Fig. 1 in the main text, we can explicitly calculate the final joint particle-detector state. The detector, which is described as a quantum harmonic oscillator, is initialized in a vacuum photon state $|0\rangle_{\rm ph}$ while the particle is initialized in the qubit $|0\rangle$ state. The particle in state $|0\rangle$ that interacts with the detector does not change the state in the cavity, while the particle in state $|1\rangle$ displaces the cavity state by g which defines the "measurement strength". This can be described as a conditional displacement operator that is written as $CD(g) \equiv |0\rangle\langle 0| \otimes I + |1\rangle\langle 1| \otimes D(g)$, where $D(g)$ is a displacement operator.

$$\begin{aligned} |\psi_f\rangle &= H \cdot CD(g) \cdot H|0\rangle|0\rangle_{\rm ph} \\ &= \frac{1}{2}|0\rangle\left(|0\rangle_{\rm ph} + |g\rangle_{\rm ph}\right) + \frac{1}{2}|1\rangle\left(|0\rangle_{\rm ph} - |g\rangle_{\rm ph}\right). \end{aligned} \tag{8}$$

In the case of a "memory-less" detector, the cavity state is reset or decoheres before an additional particle arrives, which can be described by tracing out the cavity state, in which case the particle state will reduce to be a density matrix. To evaluate the trace, we use the well-known property of coherent states $\langle\beta|\alpha\rangle = e^{-\frac{1}{2}\left(|\beta|^2+|\alpha|^2-2\beta^*\alpha\right)}$:

$$\sum_n \langle n|0\rangle\,\langle g|n\rangle = \sum_n \langle g|n\rangle\,\langle n|0\rangle = \langle g|0\rangle = e^{-\frac{1}{2}|g|^2}. \tag{9}$$

And so:

$$\rho_f = \frac{1}{2}\begin{pmatrix} 1+e^{-\frac{1}{2}|g|^2} & 0 \\ 0 & 1-e^{-\frac{1}{2}|g|^2} \end{pmatrix}. \tag{10}$$

The purity of this state is:

$$\gamma_f = \mathrm{tr}\left(\rho_f^2\right) = \frac{1+\mathrm{e}^{-|g|^2}}{2}. \tag{11}$$

It is now clear how the coupling strength can change the quantum state of the particle from being completely pure to a completely mixed state. In an interference experiment, this will correspond to vanishing interference fringes. If we consider k particles with the detector state being reset between each of them, we would get $\rho_f^{\otimes k}$. This density matrix gives rise to a binomial distribution in the final state with the parameter $\frac{1}{2}(1+e^{-\frac{1}{2}|g|^2})$. Because of that, the probability of all the particles ending in the same final state is exponentially suppressed, even if the detector is very weak.

We would like to consider now the final state of a detector that is not "memory-less". In this case, if we have k particle qubits, the final state is given by:

$$|\psi_f\rangle = H^{\otimes k}CD(g)^{\otimes k}H^{\otimes k}|0\rangle^{\otimes k}|0\rangle_{\mathrm{ph}}. \tag{12}$$

To evaluate it, we use a few identities:

$$\begin{aligned} H\cdot CD(g)\cdot H &= H\cdot\left(|0\rangle\langle 0|\otimes I + |1\rangle\langle 1|\otimes D(g)\right)\cdot H \\ &= I\otimes\frac{I+D(g)}{2} + \sigma_x\otimes\frac{I-D(g)}{2}. \end{aligned} \tag{13}$$

$$|\psi_f\rangle = \left(I\otimes\frac{I+D(g)}{2} + \sigma_x\otimes\frac{I-D(g)}{2}\right)^{\otimes k}|0\rangle^{\otimes k}|0\rangle_{\mathrm{ph}}. \tag{14}$$

We define the non-unitary operators $\frac{I+D(g)}{2}\equiv C_{\pm}$. Importantly, they commute with each other. And so:

$$|\psi_f\rangle = \sum_{n=0}^{k}\sum_{\mathrm{perm}}|0\rangle^n|1\rangle^{k-n}\otimes C_+^n C_-^{k-n}|0\rangle_{\mathrm{ph}}. \tag{15}$$

We can see that if we finally measure n particles in the $|0\rangle$ state, the state of the detector will be given by the state $C_+^n C_-^{k-n}|0\rangle_{\mathrm{ph}}$ (up to total normalization). This is a highly entangled and complex state in the general case. The probability of this scenario can be found by calculating the norm of this state:

$$P_{n,k-n} = \left\|C_+^n C_-^{k-n}|0\rangle_{\mathrm{ph}}\right\|^2 = \frac{1}{4^k}\binom{k}{n}\sum_{j=0}^{2n}\sum_{i=0}^{2(k-n)}\binom{2n}{j}\binom{2(k-n)}{i}(-1)^j e^{-\frac{|g|^2|k-i-j|^2}{2}}. \tag{16}$$

For simplicity, we assume that g is imaginary. In this case, $D(g/2) = e^{(i|g|/\sqrt{2})\hat{p}}$, where $\hat{p}$ is a quadrature of the detector Hilbert space. Therefore, the probability is given by:

$$P_{n,k-n} = \frac{1}{\sqrt{\pi}}\int dx\cos^{2n}\left(\frac{gx}{\sqrt{2}}\right)\sin^{2(k-n)}\left(\frac{gx}{\sqrt{2}}\right)e^{-x^2/2}. \tag{17}$$

This formula exemplifies why the particles show the highly uncorrelated distribution on the screen. Since sine and cosine have zeros at different points, this integral will be highly suppressed unless n is equal to zero or to k. Another way to understand this is to look at the operator norm of the operator $C_+^n C_-^{k-n}$ (in the sense of the square root of the maximal eigenvalue of $C_-^{*(k-n)}C_+^{*n}C_+^n C_-^{k-n}$). The operator $C_-^{*(k-n)}C_+^{*n}C_+^n C_-^{k-n}$ is equal to (up to unitary transformation) $\cos^{2n}(\frac{gx}{\sqrt{2}})\sin^{2(k-n)}(\frac{gx}{\sqrt{2}})$. The maximum of the function can be found to be $\frac{n^n\cdot(k-n)^{(k-n)}}{k^k}$ and so the operator norm is $\sqrt{\frac{n^n\cdot(k-n)^{(k-n)}}{k^k}}$. This function is maximal when $n=k$, 0 and minimal when $n\sim k/2$. This implies that the post-interaction electrons will always tend to bunch together to the same final state.

We are interested to see the probability of all the particles arriving at the same detector. For example, the probability of all the particles finishing in the state $|0\rangle$ is given by:

$$P_{k,0} = \frac{1}{4^k}\sum_{i=0}^{2k}\binom{2k}{i}e^{-\frac{|g|^2|k-i|^2}{2}}. \tag{18}$$

To evaluate this probability, we take the leading term in the sum and use the Stirling approximation $\binom{2k}{k}\sim\frac{4^k}{\sqrt{\pi k}}$ and therefore:

$$P_{k,0}\approx\frac{1}{\sqrt{\pi k}}\sum_{i=0}^{2k}e^{-\frac{|g|^2 i^2}{2}}\approx\frac{1}{\sqrt{\pi k}}\sum_{-\infty}^{\infty}e^{-\frac{|g|^2 i^2}{2}} = \frac{1}{\sqrt{\pi k}}\theta_3\left(0,e^{-\frac{|g|^2}{2}}\right). \tag{19}$$

Where θ_3 is the Elliptic Theta function which converges very fast to unity for large values of g. And so, we got that the probability of all the particles arriving at the same final location falls off as the square root instead of exponentially with the number of transmitted particles. This process is akin to a quantum coin toss, where the head and tail from different tosses destructively interfere. The final state turns out to be strongly skewed in contrast to the conventional common state where half the coins are heads and half are tails.

Regardless of the measured final state of the particles, the state of the photonic mode in the detector will be a quantum (i.e., not a coherent state). One particularly interesting situation is the case when all the particles are measured in the $|0\rangle$ state (which happens with probability $P_{k,0}$). In this case, the state of the photonic mode in the detectors is:

$$\frac{1}{\sqrt{P_{k,0}}}C_+^k|0\rangle_{\mathrm{ph}}\propto(I+D(g))^k|0\rangle_{\mathrm{ph}}\propto\sum_{n=0}^{k}\binom{k}{n}|(k-n)g\rangle_{\mathrm{ph}}. \tag{20}$$

And so, the final state turns up to be a 1D grid of coherent states (with a binomial envelope) centered around $kg/2$. Such states (if displaced to be centered around 0) are the basis for the creation of states like GKP states.

In the limit of small g, we can also explore the state more analytically. Again, we assume g is pure imaginary for simplicity and get:

$$|\psi_f\rangle\propto D(kg/2)(D(-g/2)+D(g/2))^k|0\rangle_{\mathrm{ph}} = e^{(ikg\hat{x})/\sqrt{2}}\cdot\cos^k\left(\frac{g\hat{x}}{\sqrt{2}}\right)|0\rangle_{\mathrm{ph}},$$

$$\langle x|\psi_f\rangle\propto e^{(ikgx)/\sqrt{2}}\cdot\cos^k\left(\frac{gx}{\sqrt{2}}\right)e^{-x^2/2}\approx e^{(ikgx)/\sqrt{2}}\cdot e^{-((k|g|^2)/4+1/2)x^2}. \tag{21}$$

And so, the resulting state is still approximately a Gaussian state, specifically a squeezed displaced state. The state is displaced along the p axis and is squeezed in x. The squeezing can then be evaluated to be:

$$e^{-((k|g|^2)/4+1/2)x^2} \equiv e^{-x^2/2e^{2r}} = \psi_{\text{squeezed}}(x)$$

$$r = \frac{1}{2}\ln\left(\frac{k|g|^2}{2}+1\right). \tag{22}$$

And the probability to post-select (calculated from the norm of the state $C_+^k|0\rangle_{\text{ph}}$) is:

$$P(r) = \frac{1}{\sqrt{\pi}}\int dx\, e^{-((k|g|^2)/2+1)x^2} = \frac{1}{\sqrt{(k|g|^2)/2+1}} = e^{-r}. \tag{23}$$

Remarkably, to obtain a given squeezing r, the number of particles required depends on the coupling strength. However, the probability to obtain this squeezing does not and is only a property of the squeezing strength.

Another particularly interesting state of the photonic mode which can be generated using conditional displacement operators is GKP states. In recent work[32], we proposed a way to generate optical GKP states using free electrons. There we showed that finite-sized '0' GKP with 10dB squeezing can be written as:

$$|0_{\text{GKP}}\rangle_{\text{ph}} \propto (D(\pi/2)+D(-\pi/2))^3 S(r=1.15,\theta=0)|0\rangle_{\text{ph}}, \tag{24}$$

where $S(\xi)$ is a squeezing operator[17]. We will now show that the state of the photonic mode from Eq. (20) with 3 electrons is equivalent to this state up to Gaussian operators, i.e., $(I+D(g))^3|0\rangle_{\text{ph}} \propto D(\alpha)S(\xi)|0_{\text{GKP}}\rangle_{\text{ph}}$ for some g, ξ, α (all taken to be real). We use some identities of squeezing and displacement operators:

$$\begin{aligned} D(\alpha)S(\xi)|0_{\text{GKP}}\rangle_{\text{ph}} &= D(\alpha)S(\xi+1.15)S(-1.15)\left(D(\sqrt{\pi/2})+D(-\sqrt{\pi/2})\right)^3 S(1.15)|0\rangle_{\text{ph}} \\ &= D(\alpha)S(\xi+1.15)\left(D(\sqrt{\pi/2}e^{1.15})+D(-\sqrt{\pi/2}e^{1.15})\right)^3|0\rangle_{\text{ph}} \\ &= D(\alpha)S(\xi+1.15)D(-\sqrt{9\pi/2}e^{1.15})\left(D(\sqrt{2\pi}e^{1.15})+I\right)^3|0\rangle_{\text{ph}}. \end{aligned} \tag{25}$$

We take $\xi=-1.15$, $\alpha=\sqrt{9\pi/2}e^{1.15}$ and get that $g=\sqrt{2\pi}e^{1.15}$. And if the interaction strength would be equal to $\sqrt{2\pi}e^{1.15}$ and we post-select 3 particles on the "even" state, we will be left with a state that is only one displacement and squeezing away from being a 10 dB GKP state:

$$S(-\xi)D(-\alpha)(I+D(g))^3|0\rangle_{\text{ph}} \propto |0_{\text{GKP}}\rangle_{\text{ph}}. \tag{26}$$

The probability to post-select this state according to Eq. (18) would be 31.3%.

As we have shown, the final state of the particles and the detectors is highly entangled. However, if we trace out the detector, the particles will remain in a mixed state, creating their state highly correlated but classically. It is a long-standing goal to achieve controllable multi-partite entanglement of many particles. This can potentially be achieved by performing measurements on the detector to collapse the joint state into a multi-partite entangled state including only the particles. Since the particle state is highly anti-correlated, such states could resemble useful states such as GHZ or highly squeezed states. To exemplify this concept, we consider the situation of 2 particles with the initial state $|00\rangle$ interacting with the detector. The final state of the joint system is given by:

$$\begin{aligned} |\psi_f\rangle = &\frac{1}{4}|00\rangle\left(|0\rangle_{\text{ph}}+2|g\rangle_{\text{ph}}+|2g\rangle_{\text{ph}}\right) \\ &+\frac{1}{4}|11\rangle\left(|0\rangle_{\text{ph}}-2|g\rangle_{\text{ph}}+|2g\rangle_{\text{ph}}\right) \\ &+\frac{1}{4}(|01\rangle+|10\rangle)\left(|0\rangle_{\text{ph}}+|2g\rangle_{\text{ph}}\right). \end{aligned} \tag{27}$$

We can define the two following states:

$$|\,\text{Bell}\,\rangle = \frac{1}{\sqrt{2}}(|00\rangle+|11\rangle),$$

$$|H\rangle = \frac{1}{2}(|00\rangle+|11\rangle+|01\rangle+|10\rangle). \tag{28}$$

We can see that if we measure the detector state in the coherent basis (via Homodyne or photon number resolving detection) and if g is large enough, then with probability 50% the state $|g\rangle$ will be measured and the particles will collapse to a Bell state $|\,\text{Bell}\,\rangle$, and with a probability of 50%, the states $|0\rangle$ or $|2g\rangle$ will be measured and the particles will collapse into the equally populated state (Hadamard state) $|H\rangle$. Since $|H\rangle$ satisfies the standard quantum limit and $|\,\text{Bell}\,\rangle$ satisfies the Heisenberg limit, the state we obtained falls somewhere in between, beating the standard quantum limit.

Quantum electron-photon interactions

In this sub-section, we briefly go over the derivation of the quantum interaction between swift electrons and quantized photonic modes. Under the paraxial approximation (i.e., assuming that the electron has a constant velocity, and that the energy of the electron is much greater than that of the photon such that the electron's dispersion can be linearized), the Hamiltonian describing the interaction between free electrons and quantized photonic modes in the Coulomb gauge ($\nabla\cdot\mathbf{A}=0$) is given by:

$$H = -i\hbar v\cdot\partial_z + \sum_n \hbar\omega_n a_n^\dagger a_n + \sum_n ev A_{n,z}(z)e^{ik_n z}\cdot a_n + ev A_{n,z}^*(z)e^{-ik_n z}a_n^\dagger. \tag{29}$$

Here, v is the velocity of the electron which is taken to propagate along the z axis, ω_n and k_n are the angular frequency and wavenumber of the n-th photonic mode, $A_{n,z}(z)$ is the projection on the z axis of the amplitude of the quantized vector potential of the n-th photonic mode; a_n, $a_n^\dagger$ are the creation and annihilation operators of the n-th mode.

We move to the interaction picture, by taking $H_0 = -i\hbar v\cdot\partial_z + \sum_n \hbar\omega_n a_n^\dagger a_n$ as the free Hamiltonian:

$$i\hbar\frac{\partial|\Psi\rangle_I}{\partial t} = V_I|\Psi\rangle_I, \tag{30}$$

where $|\Psi\rangle_I$ is the joint electron-photon wavefunction in the interaction picture and

$$V_I = \sum_n ev\left(A_{n,z}(z+vt)e^{-i\omega t+ik_n(z+vt)}\cdot a_n + A_{n,z}^*(z+vt)e^{i\omega t-ik_n(z+vt)}a_n^\dagger\right). \tag{31}$$

The solution of Eq. (30) at long times can be written as a Magnus expansion[48], and we get the scattering matrix:

$$S = \exp\left(\sum_{k=1}^{\infty}\Omega_k\right), \tag{32}$$

where for the case of Eq. (30) only the first two Ω_1 and Ω_2 are non-zero:

$$\Omega_1 = -\frac{i}{\hbar}\int_{-\infty}^{+\infty} dt\, V_I(t),$$
$$\Omega_2 = -\frac{i}{\hbar}\int_{-\infty}^{+\infty}\int_{-\infty}^{+\infty} dt_1\, dt_2\, [V_I(t_1), V_I(t_2)]. \tag{33}$$

Importantly, Ω_2 gives only the global phase and thus, we can take into account only Ω_1, $S = \exp(\Omega_1)$, where:

$$\Omega_1 = -\frac{i}{\hbar}\int_{-\infty}^{+\infty} dt \sum_n ev\left(A_{n,z}(z+vt)e^{-i\omega t+ik_n(z+vt)}\cdot a_n + A^*_{n,z}(z+vt)e^{i\omega t-ik_n(z+vt)}a_n^\dagger\right). \tag{34}$$

We change the variable inside the integral to $x = z + vt$ and get:

$$\Omega_1 = \sum_n \left(g_n a_n b_n^\dagger - g_n^* a_n^\dagger b_n\right), \tag{35}$$

where $g_n = -\frac{i}{\hbar}e\int_{-\infty}^{+\infty} A_{n,z}(\xi)e^{i(k_n-\xi/v)\xi}\, d\xi$, and the energy shift operators for the electron are:

$$b_n = e^{-i\omega_n z/v}, \quad b_n^\dagger = e^{i\omega_n z/v}. \tag{36}$$

We note that in the paraxial approximation the operator b_n decreases the energy of the electron by $\hbar\omega_n$. Thus, the final scattering matrix equals[46]:

$$S = \exp\left(\sum_n \left(g_n a_n b_n^\dagger - g_n^* a_n^\dagger b_n\right)\right). \tag{37}$$

We show how the scattering matrix of the electron-photon interaction can be represented as a conditional displacement operator and under which conditions this approximation is justified. First, we consider the case of a single photonic mode in Eq. (37), where the coupling to one of the modes is significantly stronger than the others. Then it is convenient to represent the scattering matrix as a displacement operator:

$$S = e^{gba^\dagger - g^* b^\dagger a} \equiv D(gb). \tag{38}$$

Where b is the momentum/energy displacement operator defined by Eq. (36).

In our work, we discuss the limit where the photon emission has no recoil on the particle. When the particle emits N photons, its momentum is shifted N times, the no recoil condition in this situation reads:

$$|\langle\psi_e|b^N|\psi_e\rangle|^2 \approx 1. \tag{39}$$

For a Gaussian particle shape with standard deviation of σ_z, this is equivalent to:

$$e^{-\frac{N\omega^2\sigma_z^2}{2v^2}} \approx 1 \rightarrow \sigma_z \ll \frac{v}{N\omega}. \tag{40}$$

This condition is equivalent to requiring that the extent of the particle wave function is significantly shorter than the wavelength divided by the number of photons. In our experiment, if we have k particles, they will emit a total of $(kg)^2$ photons, and so our condition on the spatial duration of the particles is:

$$\sigma_z \ll \frac{v}{\omega(kg)^2}. \tag{41}$$

Under this no recoil approximation, we can write $b \approx e^{i\phi}$ where ϕ is a constant that can be absorbed by g. We further assume that all the particles are sufficiently close together such that ϕ is the same for all of them, or that they arrive at the detector periodically with the frequency of the photon (which can be gated electrically for microwave frequency). In both cases, the scattering matrix becomes a displacement operator that depends on g:

$$S \approx D(g). \tag{42}$$

We now consider the situation where we split the particle into two trajectories such that only one of them $|1\rangle$ interacts with the detector, while the other trajectory corresponding to state $|0\rangle$ is far from the detector such that there is no interaction. We can describe the coupling to the detector g as an operator in this qubit Hilbert space, $g \rightarrow \frac{(\sigma_z+I)}{2}\cdot g$. In this case, the scattering matrix can be written as:

$$S \approx e^{g\frac{(\sigma_z+I)}{2}a^\dagger - g^*\frac{(\sigma_z+I)}{2}a} = D\left(\frac{g}{2}\right)\cdot D\left(\frac{\sigma_z g}{2}\right). \tag{43}$$

Which can be written as the conditional displacement operator:

$$S \approx |0\rangle\langle 0|\otimes I + |1\rangle\langle 1|\otimes D(g) \equiv CD(g). \tag{44}$$

Since a high-fidelity electron beam-splitter is currently out of reach, it is interesting to see how the experimental result is modified by replacing the interferometric two-port output with a traditional electron interference experiment. In the normal interferometric output case, the measurement can be understood as a projective measurement into the electron's state $|\pm\rangle$. However, when the electron's state is interfered onto a screen, the states correspond to an interference pattern on the screen with the general shape of an interference of two plane waves with wavenumber k and each one with angle $\pm\theta$ relative to the optical axis is:

$$S_+ = N\cdot\cos^2(k\theta x)$$
$$S_- = N\cdot\sin^2(k\theta x), \tag{45}$$

with N being the normalization constant. There is significant overlap between these two patterns, and so an interference experiment cannot "separate" between them like a beam splitter, making the predicted correlations challenging to observe. However, the interference patterns are somewhat separated as their peaks and troughs are onto each other, and so we can imagine tiling the measurement screen in different colors such that the areas $\pi m - \pi/4 < k\theta x < \pi/4 + \pi m$ for any integer m are associated with one interferometric output (the "+" output), and the rest are associated with the other. In the "which-path" variation with an incoherent detector, all the x's are equally likely, and so the two outputs have a 50–50 chance as usual, resulting in the ordinary binomial distribution. However, in general, if the electron is expected to go into the "+" output, its chances of going into the "+" output in the interference experiment are given by:

$$\frac{2}{\pi}\int_{-\pi/4}^{+\pi/4}\cos^2(x)\, dx = \frac{1}{2}+\frac{1}{\pi}. \tag{46}$$

And so, if in the interferometric experiment there are n electrons going to the "+" and m electrons going to the "-", then in the interference experiment the n electrons will distribute binomially into "+" with the binomial distribution $\frac{1}{2}+\frac{1}{\pi}$ and the m electrons will distribute binomially into "+" with the binomial distribution $\frac{1}{2}-\frac{1}{\pi}$. To calculate such kinds of probabilistic results, the Poisson-Binomial[37] distribution can be used. This will cause "smearing" of the observed anti-correlations as presented in Fig. 3 in the main text.

Waveguide QED

In this section, we will show how a waveguide-QED platform can be used to implement the protocol. We consider N emitters along the x axis coupled to a one-dimensional waveguide driven by lasers. The emitters have two

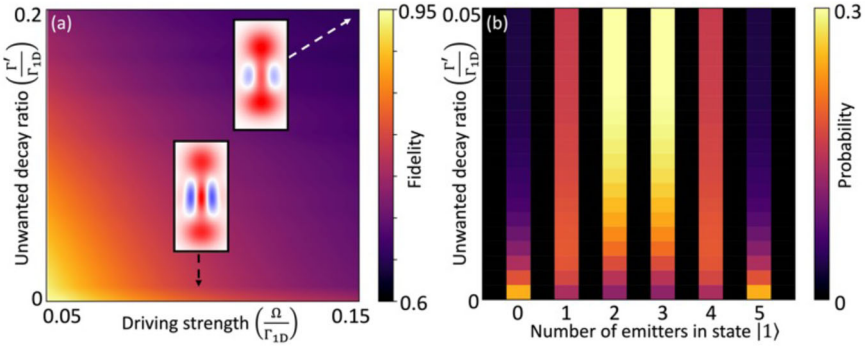

Fig. 5 | Robustness of quantum photonic state generation and correlated emitter states. a Fidelity of the emitted Schrodinger cat state in the most occupied temporal mode as a function of driving strength and unwanted decay rate. Strong driving brings the emitter into its nonlinear regime producing multiple temporal modes which hinders the fidelity of the cat state. Unwanted decays effectively measure the state of the emitter reducing the fidelity as well. The Wigner functions of generated photonic states are plotted as insets. **b** Probability for a number of emitters to finish in the state $|1\rangle$ as a function of the unwanted decay rate. Large unwanted decays measure if the emitters are in the state $|0\rangle$ or $|1\rangle$ reducing the distribution to a binomial distribution as in the case of a classical detector.

hyperfine ground levels $|0\rangle, |1\rangle$ and an excited state $|e\rangle$; the decay $|e\rangle \rightarrow |1\rangle$ is allowed while the decay $|e\rangle \rightarrow |0\rangle$ is forbidden (e.g., by selection rules). To ensure unidirectional emission, a mirror is placed at $x = 0$. A single emitter decays into the waveguide at a rate Γ_{1D} and into free space at a rate Γ'.

The equation of motion for the emitters is given by[15]:

$$\dot{\rho} = -i[H_S, \rho] + D[\sqrt{\Gamma_{1D}}S_-]\rho + \sum_n D[\sqrt{\Gamma'}\sigma_n^-]\rho, \tag{47}$$

where the Hamiltonian is $H_S = \Omega S_x - \frac{i\Gamma_{1D}}{4}\sum_{j\neq k}\left(e^{ik_0|x_k - x_j|} - e^{ik_0(x_k + x_j)}\right)\sigma_+^k\sigma_-^j$ which contains the laser driving and the coherent "flip-flop" interactions mediated by the one-dimensional waveguide. The dissipator $D[L]\rho = L\rho L^\dagger - \frac{1}{2}\{L^\dagger L, \rho\}$ describes the decay of the emitters into the waveguide. In all that follows, we assume that the emitters' locations are $x_n = (n\lambda + 1/2)$ and the Hamiltonian simplifies to $H_S = \Omega S_x$.

Our first goal is to find the radiation eigenmodes, for example, whether the emission is well described by a single temporal mode or not. Mathematically we define a creation operator for the mode as $a_0^\dagger = \int_{-\infty}^{\infty} dt'\, v_0(t')a^\dagger(t')$, with $[a(t), a^\dagger(t')] = \delta(t - t')$ and the single mode pure state as[55]:

$$|\psi_{SM}\rangle = \sum_n \frac{C_n (a_0^\dagger)^n}{\sqrt{n!}}|0\rangle. \tag{48}$$

The function $v(t')$ is normalized as $\int_{-\infty}^{\infty} dt'\, |v_0(t')|^2 = 1$, ensuring the bosonic commutation relation for $[a_0, a_0^\dagger] = 1$. If the density matrix in the most occupied temporal mode has a high fidelity to $|\psi_{SM}\rangle\langle\psi_{SM}|$, then it is well described as a single mode state.

An efficient decomposition of the output radiation into temporal modes is given by diagonalizing the first-order coherence function:

$$g^{(1)}(t_1, t_2) = \langle a^\dagger(t_1)a(t_2)\rangle = \sum_i n_i v_i^*(t_1)v_i(t_2), \tag{49}$$

where n_i is the average number of photons in the mode v_i. To calculate $g^{(1)}(t_1, t_2)$ we utilize input-output theory, which for waveguide-QED in the case considered, takes the form[56,57]:

$$a_{\text{out}}(t) = a_{\text{in}} - i\sqrt{\Gamma_{1D}}S_-(t). \tag{50}$$

This allows solving for $g^{(1)}(t_1, t_2)$ with a quantum regression theorem approach[58].

We are further interested in the joint evolution of a single temporal mode $v(t)$ and the quantum emitters. To model the quantum state of the emission, we utilize the input-output theory for quantum pulses[59], which allows for calculating the output quantum state of the photonic mode in a single temporal mode with a single master equation, which reads:

$$\dot{\rho} = -i[H_S + H_I, \rho] + D[\sqrt{\Gamma_{1D}}S_- + g_0^* a_0]\rho + \sum_n D[\sqrt{\Gamma'}\sigma_-^n]\rho, \tag{51}$$

where ρ is the joint density matrix of the emitters and the mode $v(t)$, $H_I = \frac{i\sqrt{\Gamma_{1D}}}{2}\left(g_0^*(t)a_0 S_+ - g_0(t)a_0^\dagger S_-\right)$, $g_0(t) = -v_0^*(t)\left(\int_{-\infty}^{t}|v_0(t')|^2 dt'\right)^{-1/2}$. In the limit of weak driving $\beta \equiv \frac{\Omega}{N\Gamma_{1D}} \ll 1$, the driving pulse acts as a conditional displacement on the emitters and the single mode pulse of emitted photons. We will show this below both analytically with approximations, and in numerical calculations investigating the validity of these approximations.

To analytically solve the problem, we assume that the number of excitations is much smaller than the number of emitters, which is valid in the weak drive limit: $\beta \equiv \frac{\Omega}{N\Gamma_{1D}} \ll 1$. In this limit, we can make the Holstein-Primakoff approximation[60] to exchange the collective spin raising and lowering operators S_+, S_- with bosonic operators $c^\dagger, c$ with commutation $[c, c^\dagger] = 1$. The steady state solution of the Lindblad equation for the state of the emitters in this limit is a coherent state $\rho = |\alpha\rangle\langle\alpha|$ with $\alpha(t) = \frac{i\Omega(t)}{\Gamma_{1D}}$. This allows a simple solution for the first-order coherence function:

$$g^{(1)}(t_1, t_2) = \Gamma_{1D}\langle S_+(t_1)S_-(t_2)\rangle = \Gamma_{1D}\alpha^*(t_1)\alpha(t_2). \tag{52}$$

which shows that the output is a single mode by comparing to Eq. (49).

Since the emission is single mode, the dissipator $D[\sqrt{\Gamma_{1D}}S_- + g_0^* a_0]\rho$ describing the emission into other temporal modes vanishes and we are left with a closed system evolution described by the Hamiltonian: $H_I \approx \frac{i}{2}\sqrt{\Gamma_{1D}}(g_0^*(t)S_- a_0^\dagger - g_0(t)S_+ a_0)$. If the system is constantly pumped to an eigenstate $|\alpha\rangle$ of S_-, then H_I takes the form: $H_I \approx \frac{i}{2}\sqrt{\Gamma_{1D}}(g_0^*(t)\alpha a_0^\dagger - g_0(t)\alpha^* a_0)$. The unitary time evolution operator is now a displacement operator:

$$U(t) \approx \exp\left(-\frac{1}{2}\sqrt{\Gamma_{1D}}\int_0^{t'} dt'(g_0^*(t')\alpha a_0^\dagger - g_0(t')\alpha^* a_0)\right). \tag{53}$$

We now go beyond the Holstein-Primakoff approximation[58] and solve numerically for the state of the emitters and the quantum state in the most populated mode $v_0(t)$. First, we consider the creation of a Schrödinger cat state by a single emitter in Fig. 5a. In this case, if the weak drive limit does not hold then the emission has multiple temporal modes, and the fidelity of the Schrödinger cat state in the most occupied mode is reduced, while weakly driving the emitter will prolong the emission time of the coherent state. In

addition, if there is emission into other spatial modes, the fidelity will also be reduced. One therefore would like to minimize Γ'/Γ_{1D} as much as possible.

In Fig. 5b, we study how unwanted decays of the emitters outside the waveguide alter the probability distribution between the states $|0\rangle$ and $|1\rangle$. Unwanted decays are classical detectors since they distinguish between emission from the different emitters. Thus, strong unwanted decays produce binomial distributions in the emitter states, as seen in the top rows of Fig. 5b.

Data availability

We do not analyse or generate any datasets, because our work proceeds within a theoretical and mathematical approach. One can obtain the relevant materials from the references below.

Code availability

The code used in this study is available from the corresponding author upon reasonable request.

Received: 18 June 2024; Accepted: 3 October 2024;
Published online: 21 November 2024

References

1. Young, T. The Bakerian lecture. Experiments and calculation relative to physical optic. *Phil. Trans. R. Soc.* **94**, 1 (1804).
2. Thomson, G. P. & Reid, A. Diffraction of cathode rays by a thin film. *Nature* **119**, 890 (1927).
3. Merli, P. G. et al. On the statistical aspect of electron interference phenomena. *Am. J. Phys.* **44**, 306 (1976).
4. Carnal, O. & Mlynek, J. Young's double-slit experiment with atoms: a simple atom interferometer. *Phys. Rev. Lett.* **66**, 2689 (1991).
5. Durr, S. et al. Origin of quantum-mechanical complementarity probed by a 'which-way' experiment in an atom interferometer. *Nature* **396**, 33 (1998).
6. Aharonov, Y. et al. How the result of measurement of a component of the spin of a spin-1/2 particle can turn out to be 100. *Phys. Rev. Lett.* **60**, 1351 (1988).
7. Durr, S. et al. Origin of quantum-mechanical complementarity probed by a 'which-way' experiment in an atom interferometer. *Nature* **395**, 33–37 (1998).
8. Jacques, V. et al. Experimental realization of wheeler's delayed-choice gedanken experiment. *Science* **315**, 5814 (2007).
9. Kim, Y. H. et al. Delayed 'choice' quantum eraser. *Phys. Rev. Lett.* **84**, 1 (2000).
10. Walborn, S. P. et al. Double-slit quantum eraser. *Phys. Rev. A.* **65**, 033818 (2008).
11. Feynman, R. et al. The Feynman lectures on physics. *Physics Today* **17**, 45 (1964).
12. Nielsen, M. A. & Chuang, I. *Quantum Computation and Quantum Information* Anniversary edition, Vol. 702 (Cambridge University Press, 2002).
13. Childs, A. M. Universal computation by quantum walk. *Phys. Rev. Lett.* **102**, 18 (2009).
14. Gross, M. & Haroche, S. Superradiance: An essay on the theory of collective spontaneous emission. *Phys. Rep.* **93**, 301 (1982).
15. Sheremet, A. S. et al. Waveguide quantum electrodynamics: collective radiance and photon-photon correlations. *Rev. Mod. Phys.* **95**, 015002 (2023).
16. Eickbusch, A. et al. Fast universal control of an oscillator with weak dispersive coupling to a qubit. *Nat. Phys.* **18**, 1464–1469 (2022).
17. Gerry, C. and Knight, P. L. *Introductory Qantum Optics,* Vol. 332 (Cambridge University Press, 2005).
18. Lin, C. Y. et al. Encoding qubits into harmonic-oscillator modes via quantum walks in phase space. *Quant. Inf. Process.* **19**, 272 (2020).
19. Kuzmich, A. et al. Atomic quantum non-demolition measurements and squeezing. *EPL* **42**, 481 (1998).
20. Sørensen, A. & Mølmer, K. Probabilistic generation of entanglement in optical cavities. *Phys. Rev. Lett.* **90**, 12 (2003).
21. Madsen, L. & Mølmer, K. Spin squeezing and precision probing with light and samples of atoms in the Gaussian description. *Phys. Rev. A.* **70**, 052324 (2004).
22. Vasilakis, G. et al. Generation of a squeezed state of an oscillator by stroboscopic back-action-evading measurement. *Nat. Phys.* **11**, 389–392 (2015).
23. Boto, A. N. & al, et Quantum interferometric optical lithography: exploiting entanglement to beat the diffraction limit. *Phys. Rev. Lett.* **85**, 2733 (2000).
24. Okamoto, H. Possible use of a cooper-pair box for low-dose electron microscopy. *Phys. Rev. A.* **85**, 043810 (2013).
25. Okamoto, H. & Nagatani, Y. Entanglement-assisted electron microscopy based on a flux qubit. *Appl. Phys. Lett.* **104**, 062604 (2014).
26. Okamoto, H. Measurement errors in entanglement-assisted electron microscopy. *Phys. Rev. A.* **89**, 063828 (2014).
27. Kruit, P. et al. Designs for a quantum electron microscope. *Ultramicroscopy.* **164**, 31–45 (2016).
28. Koppell, S. A. et al. Transmission electron microscopy at the quantum limit. *Appl. Phys. Lett.* **120**, 190502 (2022).
29. Wigner, E. P. On the quantum correction for thermodynamic equilibrium. *Phys. Rev.* **40**, 103, (1932).
30. Gottesman, D. et al. Encoding a qubit in an oscillator. *Phys. Rev. A.* **64**, 012310 (2001).
31. Bourassa, J. E. et al. Blueprint for a scalable photonic fault-tolerant quantum computer. *Quantum* **5**, 392 (2021).
32. Dahan, R. et al. Creation of optical cat and GKP states using shaped free electrons. *Phys. Rev. X.* **13**, 031001 (2023).
33. Tonomura, A. Applications of electron holography. *Rev. Mod. Phys.* **59**, 639 (1987).
34. Cowley, J. M. Twenty forms of electron holography. *Ultramicroscopy.* **41**, 4 (1992).
35. Lichte, H. & Lehmann, M. Electron holography-basics and applications. *Rep. Prog. Phys.* **71**, 016102 (2008).
36. Tanigaki, T. et al. Split-illumination electron holography. *Appl. Phys. Lett.* **101**, 043101 (2012).
37. Fernandez, M. & Williams, S. Closed-form expression for the poisson-binomial probability density function. *IEEE. Tran. Aerosp. Electron. Syst.* **46**, 2 (2010).
38. Marton, L. et al. Electron beam interferometer. *Phys. Rev.* **90**, 490 (1953).
39. Mertens, B. M. et al. Off-axis holography with a crystal beam splitter. *Ultramicroscopy.* **77**, 1–2 (1999).
40. Harvey, T. R. et al. Interpretable and efficient interferometric contrast in scanning transmission electron microscopy with a diffraction-grating beam splitter. *Phys. Rev. Appl.* **10**, 061001 (2018).
41. Turner, A. E. et al. Interaction-free measurement with electrons. *Phys. Rev. Lett.* **127**, 110401 (2021).
42. Dellweg, M. M. & Muller, C. Spin-polarizing interferometric beam splitter for free electrons. *Phys. Rev. Lett.* **118**, 070403 (2017).
43. Hammer, J. et al. Microwave chip-based beam splitter for low-energy guided electrons. *Phys. Rev. Lett.* **114**, 254801 (2015).
44. Yang, Y. et al. Efficient two-port electron beam splitter via a quantum interaction-free measurement. *Phys. Rev. A.* **98**, 043621 (2018).
45. Huang, G. et al. Electron-photon quantum state heralding using photonic integrated circuits. *PRX Quant.* **4**, 020351 (2023).
46. Kfir, O. Entanglement of electrons and cavity photons in the strong-coupling regime. *Phys. Rev. Lett.* **123**, 103602 (2019).
47. Giulio, V. D. et al. Probing quantum optical excitations with fast electrons. *Optica.* **6**, 12 (2019).
48. Magnus, W. On the exponential solution of differential equations for a linear operator. *Comm. Pure Appl. Math*. **7**, 649–673(1954).

49. Feist, A. et al. Cavity-mediated electron-photon pairs. *Science.* **377**, 6607 (2022).
50. Adiv, Y. et al. Observation of 2D cherenkov radiation. *Phys. Rev. X.* **13**, 011002 (2023).
51. Yan, Q. et al. Single-particle-single-photon coupling using a circuital metamaterial cavity. *Tech. Digest Series.* https://doi.org/10.1364/CLEO_FS.2023.FF3D.1 (2023).
52. Sonnentag, P. & Hasselbach, F. Measurement of decoherence of electron waves and visualization of the quantum-classical transition. *Phys. Rev. Lett.* **98**, 200402 (2007).
53. Kerker, N. et al. Quantum decoherence by Coulomb interaction. *New. J. Phys.* **22**, 063039 (2020).
54. Vitanov, N. V. et al. Stimulated Raman adiabatic passage in physics, chemistry, and beyond. *Rev. Mod. Phys.* **89**, 015006 (2017).
55. Fabre, C. Modes and states in quantum optics. *Rev. Mod. Phys.* **92**, 035005 (2020).
56. Gardiner, C. W. & Collett, M. J. Input and output in damped quantum systems: quantum stochastic differential equations and the master equation. *Phys. Rev. A* **31**, 3761–3774 (1980).
57. Caneva, T. et al. Quantum dynamics of propagating photons with strong interactions: a generalized input-output formalism. *New J. Phys.* **17**, 113001 (2015).
58. Gardiner, C.W. and Zoller, P. *Quantum Noise: A Handbook of Markovian and Non-Markovian Quantum Stochastic Methods with Applications to Quantum Optics* 3rd ed. 2004 edition, Vol. 450 (Springer Science & Business Media, 2004).
59. Kiilerich, A. & Mølmer, K. Input-output theory with quantum pulses. *Phys. Rev. Lett.* **123**, 123604, (2019).
60. Holstein, T. & Primakoff, H. Field dependence of the intrinsic domain magnetization of a ferromagnet. *Phys. Rev.* **58**, 1098 (1940).
61. Neeley, M. et al. Generation of three-qubit entangled states using superconducting phase qubits. *Nature* **467**, 570–573 (2010).
62. Rauschenbeutel, A. et al. Step-by-step engineered multiparticle. *Science* **288**, 2024–2028 (2000).
63. Cirac, J. I. & Zoller, P. Quantum computations with cold trapped ions. *Phys. Rev. Lett.* **74**, 4091 (1995).
64. Sørensen, A. & Mølmer, K. Quantum computation with ions in thermal motion. *Phys. Rev. Lett.* **82**, 1971 (1999).
65. Monroe, C. et al. Demonstration of a fundamental quantum logic gate. *Phys. Rev. Lett.* **75**, 4714–7 (1995).
66. Kannan, B. et al. Waveguide quantum electrodynamics with superconducting artificial giant atoms. *Nature* **583**, 775–779 (2020).
67. Kannan, B. et al. On-demand directional microwave photon emission using waveguide quantum electrodynamics. *Nat. Phys.* **19**, 394–400 (2023).
68. Tiranov, A. et al. Collective super- and subradiant dynamics between distant optical quantum emitters. *Science* **379**, 389–393 (2023).
69. Dordevic, T. et al. Entanglement transport and a nanophotonic interface for atoms in optical tweezers. *Science* **373**, 1511–1514 (2021).
70. Yan, Z. et al. Super-radiant and sub-radiant cavity scattering by atom arrays. *Phys. Rev. Lett.* **133**, 253603 (2023).
71. Chang, D. E. et al. Quantum nonlinear optics - photon by photon. *Nat. Photon.* **8**, 685–694 (2014).

Acknowledgements

We would like to thank Dr. Yonatan Israel (Tel-Aviv university, Israel) and Ms. Gefen Baranes (MIT/Harvard, USA) for fruitful discussions. This research is supported by the ADAMS fellowships program of the Israel Academy of Sciences and Humanities.

Author contributions

The original idea and it's mathematical formulation was conceived by R.R and I.K. The extension of the idea to platforms such as waveguide QED was conceived by O.T under the guidance of K.M. The mathematical derivations, analysis and scripting used in this work where all performed by R.R, O.T and A.G. The manuscript was written by R.R and O.T under the guidance of K.M and I.K.

Competing interest

The authors declare no competing interests.

Additional information

Correspondence and requests for materials should be addressed to Ido Kaminer.